June 19th, 2024

Towards accurate modeling of vibration in CFD-DEM simulations of vibrated gas-fluidized beds without using a moving mesh

Qiang Guo^{1,2*}, Jieyu Tian¹, Runsheng Huang¹, Christopher M. Boyce^{1*}

¹Department of Chemical Engineering, Columbia University, New York, New York 10027, USA ²State Key Laboratory of Mesoscience and Engineering, Institute of Process Engineering, Chinese Academy of Sciences, Beijing 100190, China

- (*) Corresponding author. Email: guoqiang@ipe.ac.cn.
- (*) Corresponding author. Email: cmb2302@columbia.edu.

Abstract

Vibrated gas-fluidized beds are widely used industrially, and two main methods exist to

simulate them computationally: (i) in a moving reference frame by oscillating gravity and (ii) in a

stationary reference frame by moving the distributor. Further, it is unclear whether gas flow in the

plenum chamber of a vibrated fluidized bed should be modeled as constant or oscillating. Here,

we challenge the accuracy of different potential modeling methods by comparing with

experimental results of structured bubbling because these results are deterministic, avoiding the

need for comparing via statistically averaged quantities. Results show that modeling a moving

distributor and moving sidewalls as physically accurately as possible is important, and modeling

the system in the moving reference frame is less accurate than in the stationary reference frame,

due to subtle differences. Further, it is more accurate to model the gas flow as constant rather than

oscillatory in the plenum chamber.

Keywords: Vibrated gas-fluidized bed; Numerical model; Structured bubbling; CFD-DEM;

Moving mesh

2

1. Introduction

A typical gas-solids fluidized bed consists of a vertical vessel confined by walls, a bed of particles, and a distributor at the bottom to provide uniform upward gas flow. Fluidization occurs when the gas flow rate (U) exceeds the minimum fluidization velocity (U_{mf}) required for upward drag force to suspend the weight of particles (Yang, 2003). In the fluidization state, particles are well mixed and rapid heat and mass transport can be achieved. Nevertheless, gas fluidization alone has a limited ability to fluidize (i) fine Geldart C (Geldart, 1973) particles due to the formation of particle agglomeration and (ii) large Geldart D (Geldart, 1973) particles due to gas channeling as a result of spatial non-uniformity of particle distribution.

Among many different methods to intensify the operation of fluidized beds, vibrated gasfluidized beds introduce external vibration, typically in the vertical direction, to provide energy to
overcome interparticle cohesive forces and break gas preferential paths. So far, vibrated gasfluidized beds have been used in a series of applications to fluidize micro-scale Geldart C particles
(Noda et al., 1998) and very fine nano-scale particles in the range of 1-100 nm (Hoorijani et al.,
2021) as well as very large particles with the size larger than 1 mm (Yang et al., 2017). In
commercial, industrial-scale units, vibrated gas-fluidized beds have been successfully used to dry
and cool food and pharmaceutical powders (Lehmann et al., 2019). Further, it has been shown that
at specific conditions, some highly predictable and ordered meso-scale structures can be formed
in vibrated gas-fluidized beds, including structured convection cells (Guo et al., 2022a), structured
bubbling (Guo et al., 2021), and structured surface waves (Guo et al., 2023b; Omidi et al., 2024).
Historically, the scale-up of fluidized beds has long been challenged by the chaotic hydrodynamics
inside the system (Chew et al., 2022). In this regard, these identified structured flow patterns
formed in vibrated gas-fluidized beds might have potential to address the challenge associated with

conventional fluidized beds, as preliminary tests in pseudo-2D systems have shown that these patterns can repeat themselves with vibration and can maintain their characteristic size with system width increased. Nevertheless, it should be noted that the evolution and reproduction of these ordered meso-scale structures in large 3D systems remains unknown at this moment. For a summary of the advances of vibrated gas-fluidized beds, the readers are referred to a recent review (Guo et al., 2023c).

Numerical modeling based on a multi-scale strategy has become a powerful tool to understand the hydrodynamics and the underlying mechanisms of fluidization in the last two decades (van der Hoef et al., 2006). As the models developed for fluidized beds are based on universal laws of physics such as the mass conservation and the Newton's second law, they can also be used in situations of vibrated gas-fluidized beds if vibration can be modeled accurately. So far, Computational Fluid Dynamics-Discrete Element Method (CFD-DEM) (Guo et al., 2021; Guo and Boyce, 2022; Hartig et al., 2022, 2021; Jiang et al., 2020; McLaren et al., 2019; Tatemoto et al., 2005, 2004; Xiang et al., 2010) and Two-Fluid Modeling (TFM) (Acosta-Iborra et al., 2012; Cano-Pleite et al., 2015; Guo et al., 2023a, 2022b; Rahimi et al., 2013) have been used to model vibrated gas-fluidized beds, and different methods have been developed to model vibration.

For a typical vertically vibrated gas-fluidized bed, the whole bed, including both the bottom distributor and sidewalls, is moving sinusoidally up and down driven by a shaker that supports the bed. Energy from the vibration is transferred to the fluidized particles through collisional interactions with the distributor and frictional contacts with the moving sidewalls (Wang et al., 2000). Ideally, to approximate the real situation, the simulated bed column should be moving, and therefore a moving mesh should be used to deal with fluid grids (**Fig. 1a**). The best aspect of using a moving CFD mesh to model vibration is that it can fully consider the change of the coordinates

of the whole bed due to vibration in the stationary reference frame. As such, vibration can be modeled fully. Such a modeling method, however, is computationally expensive (Doustdar and Kazemi, 2019) and may suffer from the consistency of the mass and momentum balances in the computational cells at the distributor (Acosta-Iborra et al., 2012). To the best knowledge of the authors, the only work that modeled vibration using a moving mesh in simulations of vibrated gas-fluidized beds with vertical vibration is by Yang et al. (2023) very recently, based on the CFD-DEM method using commercial software of ANSYS Fluent and EDEM. Another similar work was by Li et al. (2022), who adopted a moving mesh in CFD-DEM simulations of a fluidized bed with ultrasonic horizontal vibration at a very small vibration amplitude.

If methods without relying on a moving CFD mesh are used to model vibration, the effect of vibration can only be considered by virtually moving the key components in the bed, i.e., distributor and sidewalls, in an indirect manner, since the movement of the whole bed in the stationary reference frame cannot be modeled. In some early CFD-DEM simulations of vibrated gas-fluidized beds (Tatemoto et al., 2005, 2004; Xiang et al., 2010), fluid grids remain fixed to the laboratory framework and the vibrated bed moves through the computational domain by changing the size of the lowest row of fluid grids according to the position of the bottom gas inlet boundary for the distributor (**Fig. 1b**). As such, the vibration amplitude cannot exceed the size of the fluid grids. In situations without the use of the bottom gas inlet boundary (Zeilstra et al., 2008), this problem can be solved by allowing the lowest computational cells to be cut by the bottom plate and updating fluid grids that couples with the particles. Recently, inspired by the idea to "glue" particles together to model a rough wall in many pure DEM simulations (Valverde et al., 2001; Xu et al., 2017), Hartig et al. (2022) proposed to use a horizontal layer of "frit particles" located above the bottom gas inlet boundary to approximate the moving porous distributor, and at the same time,

the bottom gas inlet boundary remains fixed (**Fig. 1c**). As such, the complicated handling of vibrating the bottom gas inlet boundary in Tatemoto et al. (2005, 2004) and Xiang et al. (2010) is avoided, and thus the value of vibration amplitude is not restricted by the fluid grid size. However, as pointed by Xu et al. (2017), the use of "frit particles" to model a plate can overestimate the effect of friction. Further, the vibration of sidewalls, which also introduce energy to the system, was ignored in Hartig et al. (2022).

From another direction, Acosta-Iborra et al. (2012) proposed to model vibration via solving model equations in a coordinate reference system that moves with the vibrated gas-fluidized bed in TFM simulations (hereinafter called the moving reference frame). By the transformation, the gas and solids momentum equations are introduced to an additional acceleration term through body forces. Later, Jiang et al. (2020) extended the same idea to CFD-DEM simulations of vibrated gasfluidized beds. The effect of this modeling strategy is equivalent to model vibration by oscillating gravity according to the vibration conditions (Fig. 1d). Theoretically, this method captures the full physics of vibration because it stands on the basis of transformation of the coordinate reference system, rather than directly and explicitly models the vibration of the distributor and sidewalls in a vibrated gas-fluidized bed. Due to the simplicity without the need to change the boundary conditions, oscillating gravity has been widely used to model vibration in CFD-DEM (Guo et al., 2021; Guo and Boyce, 2022; Hartig et al., 2021; McLaren et al., 2019) and TFM (Cano-Pleite et al., 2015; Guo et al., 2023a, 2022b; Omidi et al., 2024; Rahimi et al., 2013) simulations of vibrated gas-fluidized beds. However, in all of the aforementioned methods, it is unclear exactly how gas enters the fluidized bed and thus how the gas inlet velocity should be modeled.

To sum up, there are two different approaches in the literature to model vibration in numerical simulations of vibrated gas-fluidized beds without using a moving mesh: (i) by oscillating gravity to transform the system into the moving reference frame and (ii) by moving the distributor and sidewalls to approximate a real setup. However, a comparison between these two modeling methods is lacking. This motivates us to conduct the current work based on CFD-DEM simulations. Further, beyond all previous works, we propose to model vibration by moving a flat surface that is located above the fixed bottom gas inlet boundary and only seen by DEM to mimic the vibrated distributor and also imposing a tangential velocity on the walls to mimic the movement of sidewalls (**Fig. 1e**). This proposed method is believed to provide the most accurate and direct approximation to the real vibrated gas-fluidized beds without relying on a moving mesh. Further, we conduct what to our knowledge is the first investigation of the gas inlet velocity conditions necessary to model vibrated gas-fluidized beds most accurately.

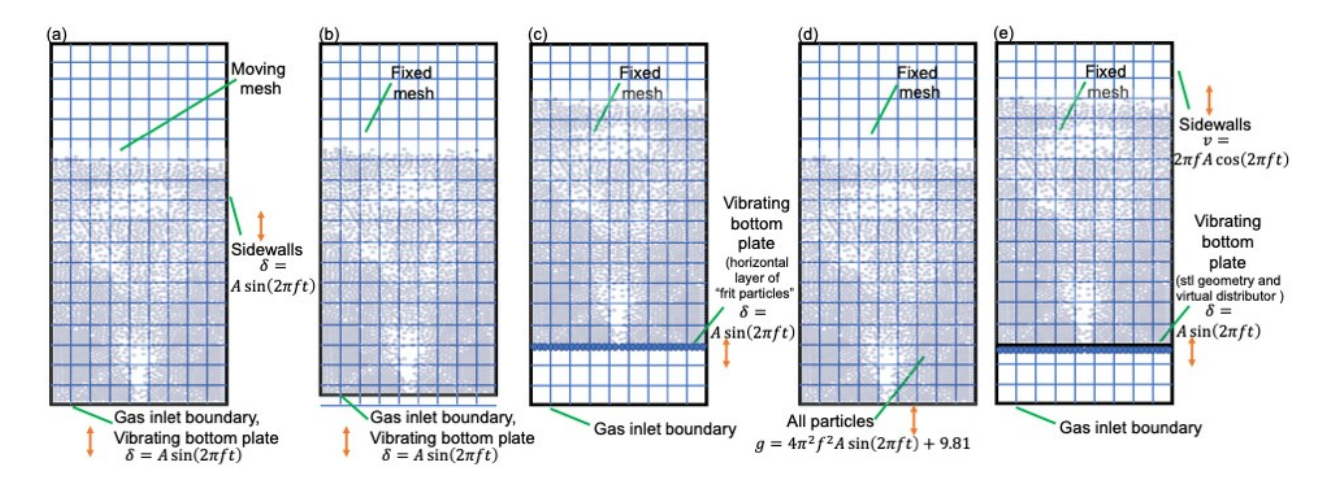


Figure 1. Schematic illustration of different vibration modeling methods in CFD-DEM simulations of vibrated gas-fluidized beds with dots showing discrete particles and squares showing gas fluid grids: (a) vibrating bottom plate and sidewalls based on a moving mesh (Yang et al., 2023); (b) the method used in (Tatemoto et al., 2005, 2004; Xiang et al., 2010) by changing the size of the bottom row of fluid grids; (c) the method used in (Hartig et al., 2022) by moving the bottom plate represented by a horizontal layer of "frit particles"; (d) the method used in (Jiang et al., 2020) to oscillate gravity; and (e) the method proposed in this work by moving a flat surface that is located above the fixed gas inlet boundary and only seen by DEM and imposing a tangential velocity on the sidewalls.

The simulation case we used to evaluate different vibration modeling methods is the structured bubbling pattern produced in a pseudo-2D vibrated gas-fluidized bed (Guo et al., 2021).

As described in Wu et al. (2017) for structured bubbling produced in pulsed fluidized beds, the pattern can serve as a simple yet robust "fingerprint" to validate simulations. This is also true for structured bubbling in vibrated gas-fluidized beds, since the triangular tessellation pattern that repeats itself periodically with vibration relies on the complex interplay of gas-solids forces and changes of granular rheology in time and space as well as vibration that creates the pattern, all of which have to be properly considered for a model to correctly predict the pattern.

The organization of this work is as follows. First, model equations, simulation setup, different modeling methods of vibration and gas inlet velocity, and data post-processing are briefly described. Then, simulation results of bubbling patterns predicted by different modeling methods for (i) the vibration and (ii) the gas inlet velocity are compared with experiments, and results are discussed. Finally, the paper ends with conclusions.

2. Methods

2.1 Model equations

All the CFD-DEM simulations performed in this work were based on MFiX (Garg et al., 2012), an open-source package developed by the National Engineering Technology Laboratory. In CFD-DEM, the motion of the gas phase is solved by the volume-averaged Navier-Stokes equations on Eulerian grids and the continuity and momentum conservation equations are:

$$\frac{\partial(\varepsilon_g \rho_g)}{\partial t} + \nabla \cdot (\varepsilon_g \rho_g \vec{\boldsymbol{u}}_g) = 0 \tag{1}$$

$$\frac{\partial (\varepsilon_g \rho_g \vec{\boldsymbol{u}}_g)}{\partial t} + \nabla \cdot \left(\varepsilon_g \rho_g \vec{\boldsymbol{u}}_g \vec{\boldsymbol{u}}_g\right) = -\varepsilon_g \nabla p_g + \nabla \cdot \bar{\boldsymbol{\tau}}_g + \varepsilon_g \rho_g \vec{\boldsymbol{g}} + \sum\nolimits_{p=1}^{N_p} \beta \frac{V_p}{V_c} (\vec{\boldsymbol{u}}_p - \vec{\boldsymbol{u}}_g) \tag{2}$$

where ε_g , p_g , and \vec{u}_g are the void fraction, pressure, and local average velocity of the gas phase, respectively, \vec{u}_p is the particle velocity, V_p is the volume of a particle, V_c is the volume of the grid, N_p is the total number of particles, and \vec{g} is the gravitational acceleration. The gas phase density ρ_g is calculated via the equation of state of an ideal gas law:

$$\rho_g = \frac{p_g M_g}{RT_g} \tag{3}$$

where M_g and T_g are the molecular weight and temperature of the gas phase, respectively, and R is the ideal gas constant. The temperature inside the bed is assumed to be a constant of 293.15 K, avoiding the addition of energy equations. The change of the gas phase density is thus due to the pressure drop and fluctuation through the bed. The stress tensor of the gas phase $\overline{\tau}_g$ is solved following the Newtonian fluid behavior:

$$\bar{\bar{\tau}}_g = \mu_g \left(\nabla \vec{\boldsymbol{u}}_g + \nabla \vec{\boldsymbol{u}}_g^T \right) - \frac{2}{3} \mu_g (\nabla \cdot \vec{\boldsymbol{u}}_g) \bar{\bar{\boldsymbol{I}}}$$
 (4)

where μ_g is the viscosity of the gas phase and \overline{I} is an identity tensor.

In CFD-DEM, the trajectory of each particle with the diameter of d_p , density of ρ_p , mass of m_p , and moment of inertia l_p is tracked by solving Newton's second law:

$$\frac{d\vec{x}_p}{dt} = \vec{u}_p \tag{5}$$

$$m_p \frac{d\vec{u}_p}{dt} = m_p \vec{g} + \vec{F}_c + \vec{F}_d \tag{6}$$

$$I_{p}\frac{d\overrightarrow{\boldsymbol{\omega}}_{p}}{dt} = \overrightarrow{\boldsymbol{T}}_{p} \tag{7}$$

where \vec{x}_p is the particle position, \vec{F}_c is the net contact force resulted from particle-particle or particle-wall interaction, \vec{F}_d is the drag force exerted by the surrounding gas phase, $\vec{\omega}_p$ is the particle angular velocity, and \vec{T}_p is the total torque acting on the particle. Note that the motion of every individual particle was explicitly tracked and the techniques developed to speed up DEM simulations (Zhang and Ge, 2024), such as coarse graining and source smoothing (Jurtz et al., 2020), were not used here.

The Hertzian model (El-Emam et al., 2021) was used to calculate \vec{F}_c , in which five interdependent parameters, including the Coulomb friction coefficient μ , Young's modulus G, Poisson's ratio σ , the normal and the tangential restitution coefficient (e_n and e_t), are needed.

The drag force \vec{F}_d summarizes the contributions from pressure gradient and viscosity, and is calculated by

$$\vec{F}_d = -V_p \nabla p_q + \beta V_p (\vec{u}_q - \vec{u}_p) \tag{8}$$

The interphase momentum exchange coefficient β in Equations 2 and 8 was closed by the Gidaspow drag law (Ding and Gidaspow, 1990):

$$\beta = \begin{cases} 150 \frac{(1 - \varepsilon_g)\mu_g}{\varepsilon_g d_p^2} + 1.75 \frac{\rho_g |\vec{u}_g - \vec{u}_p|}{d_p} & \varepsilon_g \le 0.8\\ \frac{3}{4} C_D \frac{\rho_g |\vec{u}_g - \vec{u}_p| \varepsilon_g^{-1.65}}{d_p} & \varepsilon_g > 0.8 \end{cases}$$

$$C_D = \begin{cases} 0.44 & Re > 1000\\ \frac{24}{Re} (1 + 0.15Re^{0.687}) & Re \le 1000 \end{cases}$$

$$(9)$$

$$C_D = \begin{cases} 0.44 & Re > 1000\\ \frac{24}{Re} (1 + 0.15Re^{0.687}) & Re \le 1000 \end{cases}$$
 (10)

$$Re = \frac{\rho_g \varepsilon_g d_p |\vec{\boldsymbol{u}}_g - \vec{\boldsymbol{u}}_p|}{\mu_g}$$
 (11)

where C_D is the drag coefficient and Re is the particle Reynolds number.

2.2 Simulation setup

Fig. 2a shows the schematic of the simulated setup, and for comparison, Fig. 2b shows the setup used in experiments (Guo et al., 2021). The simulated fluidized bed had a width of 200 mm and a depth of 10 mm, the same as in experiments (Guo et al., 2021). The bed height including freeboard was decreased from 500 mm in experiments to 160 mm in simulations to save the computational costs, but the fill height of particles was the same in experiments and simulations. As seen in Supporting Information Figure S1, further increasing the bed height to 240 mm or 360 mm while keeping other conditions including the CFD cell size and particle height the same as the case with a bed height of 160 mm does not significantly affect the predicted bubbling pattern, due to the fact that the freeboard region in the latter case is already high enough, which does not interfere the particle flow field in the bed. The simulated gas phase was air at atmospheric pressure with a viscosity of 1.8×10^{-5} Pa·s and a molecular weight of 29 g/mol. Two particle phases were simulated, both were spherical in shape and had a density of 2500 kg/m³. The particle phase with an ID of 1, used as the fluidized particles, had a normal distribution from 400 to 600 µm with the average of 500 µm and a standard deviation of 30 µm. The particle phase with an ID of 2 was used to model a virtual distributor and had the same size distribution as the particle phase 1. Both the properties of the gas phase and the fluidized particles were close to experiments. It has been widely accepted that the bed depth, gas phase density, and particle size distribution can significantly affect the hydrodynamics of fluidized beds (Grace et al., 2020). However, in previous CFD-DEM simulations of structured bubbling created either by pulsed gas flow (Wu et al., 2017) or vibration (Guo et al., 2021; Guo and Boyce, 2022), simplifications have been made in these three aspects by decreasing the bed depth to a thinner domain, treating the gas phase as incompressible, and using a monodisperse particle size. With this in mind, we carefully set up the simulations to match experiments by using the same bed depth as in experiments, calculating the gas phase density from an ideal gas law, and considering particle size distribution. Therefore, besides the vibration modeling approach that will be detailed below, the simulations conducted in this work are more physically accurate than previous simulations of structured bubbling.

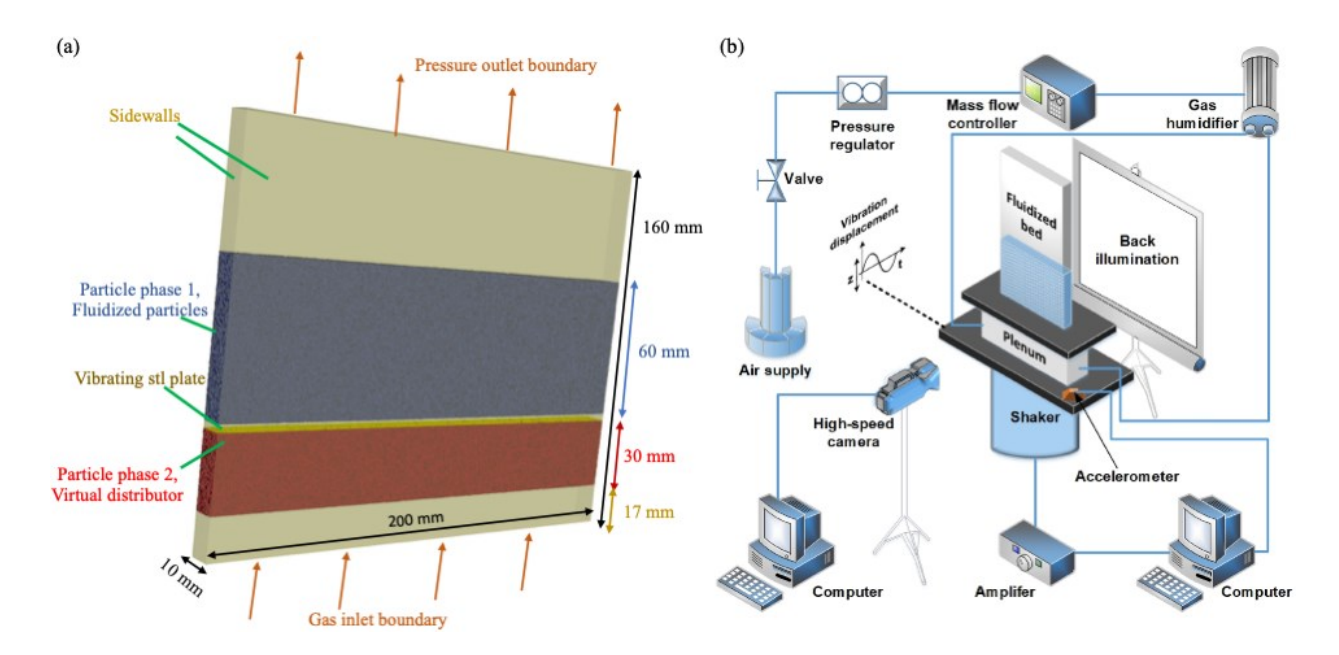


Figure 2. Schematic illustration of the setup used in (a) simulations and (b) experiments (Guo et al., 2021).

A structured CFD grids was used with the size of 2 mm in all directions, about 3.3-5.0 particle diameters in side length. Such a grid size lies in the suggested value range of 3-5 particle diameters in the literature to obtain mesh-independent solutions from CFD-DEM simulations (Peng et al., 2014; Tsuji et al., 1992). Also, there is not much space to further refine the grid size as it has been shown that if the grid size is smaller than 1.63 particle diameters, an unphysical flow field would be predicted (Peng et al., 2014).

In the experiments, gas was injected through two tubes into the plenum chamber (**Fig. 2b**) at a constant flow rate corresponding to a superficial gas velocity of 0.30 m/s, equaling $1.4U_{mf}$. The U_{mf} obtained in experiments and simulations is both 0.22 m/s. Since the plenum chamber is moved up and down on the shaker (**Fig. 2b**), it is unclear what complex gas flow patterns this could create in the plenum chamber distributor, and how this gas flow is best modeled as an inlet gas velocity in the system geometry shown in **Fig. 2a**. As such, we investigated different gas inlet conditions, as discussed further in Section 2.4.

The top outlet boundary condition was set to constant atmospheric pressure. The wall boundary condition at all the sidewalls was set to be no-slip for the gas phase and rigid wall for the particles.

Initially, at a height of 17 mm from the bottom, 532,682 randomly and closely packed particles with the phase ID 2 were fixed to model as a virtual distributor with a height of 30 mm. A movable flat surface plate is placed just above the virtual distributor. This plate is only seen by DEM and has no resistance exerted on the gas phase. The format of the plate geometry might need to be adjusted per different CFD packages and is in stereolithography (STL) format in MFiX, which features the use of movable internal surface with STL format. A total of 1,066,671 randomly and closely packed particles with the phase ID 1 and located in the region 50 mm from the bottom were used as fluidized particles, leading to a particle fill height of 60 mm, matching experiments. The placement of fluidized particles above the bottom gas inlet with a distance void of particles which models a plenum chamber, as inspired by Hartig et al. (2022), is to ensure to use a fixed location of gas inlet boundary. However, this can result in gas maldistribution through the fluidized particles. Therefore, a virtual distributor made of randomly and closely packed particles is used and located just below the movable flat surface plate. The pressure drop across the virtual distributor is about 50% of the bed pressure drop, creating a uniform gas flow distribution into the bed.

Table 1. Detailed parameters used in simulations.

Quantity	Simulations	
Bed width, mm	200	
Bed depth, mm	10	
Bed height, mm	160	
CFD mesh size, mm	2	
Gas viscosity, Pa·s	1.8×10^{-5}	
Gas molecular weight, g/mol	29	
Temperature in the bed, K	293.15	

Particle size, µm

Normal distribution from 400 to 600 μm Average: 500 μm ; Standard deviation: 30 μm

Particle density, kg/m ³	2500		
Minimum fluidization velocity, m/s	0.22		
Coulomb friction coefficient	0.35		
Young's modulus, Pa	1×10^{6}		
Poisson's ratio	0.22		
Normal restitution coefficient	0.9		
Tangential restitution coefficient	0.9		
Vibration frequency, Hz	5		
Vibration amplitude, mm	1.0, 3.0, 4.5, 6.0, 8.0		
Drag law model	Gidaspow (Ding and Gidaspow, 1990)		
Inlet boundary condition	See Table 3		
Outlet boundary condition	Atmospheric pressure		
Wall houndary condition	No-slip for gas phase;		
Wall boundary condition	Rigid wall for particle		
CFD Time step, s	1×10^{-4}		
DEM time step, s	1×10^{-6}		

The Coulomb friction coefficient μ , Young's modulus G, Poisson's ratio σ , the normal restitution coefficient e_n , and the tangential restitution coefficient e_t between all the particle-particle and particle-wall interaction were set to 0.35, 1×10^6 Pa, 0.22, 0.9, and 0.9 respectively, corresponding to the typical values used for glass beads in experiments. The simulations were run for 8 s with a time step of 1×10^{-6} s for DEM and a time step of 1×10^{-4} s for CFD. Detailed parameters used in simulations are summarized in **Table 1**.

2.3 Modeling vibration of the fluidized bed

In this section, different vibration modeling methods used in CFD-DEM simulations conducted in this work are briefly introduced. All these methods use a fixed CFD mesh and therefore the bottom gas inlet boundary is also fixed. In contrast, if a moving CFD mesh was used to model vibration, as done in the work by Yang et al. (2023), the location of the bottom gas inlet boundary changes with time, and the wall and interior CFD cells adjacent to the moving bottom gas inlet boundary need to be moved over time with periodic back-and-forth motion and updated algorithmically, which significantly complicates the simulations and prolongs the wall time needed.

For all the four tested methods, the vibration frequency f was fixed at 5 Hz, which is the same as in experiments (Guo et al., 2021), while the vibration amplitude A was varied with values

of 1.0 mm, 3.0 mm, 4.5 mm, 6.0 mm, and 8.0 mm to find a condition that produces the best structured bubbling pattern for a certain method. In experiments (Guo et al., 2021), the optimal *A* for producing structured bubbling is 4.5 mm.

The case files and user-defined functions for each vibration modeling method are provided on GitHub (https://github.com/guoq52ce/VibrationModeling/tree/main), so that others can simply test the effect of different vibration modeling methods on their simulation results of vibrated gasfluidized beds.

2.3.1 Method 1: oscillating gravity to model in the moving reference frame

Oscillating gravity is the simplest way to model vibration in numerical simulations of vibrated gas-fluidized beds (Acosta-Iborra et al., 2012; Jiang et al., 2020). In this method, both the particles in the virtual distributor and the movable flat surface are kept stationary. The gravitational acceleration in both CFD and DEM parts is changed with time following $\vec{g} = -9.81 - (2\pi f)^2 A \sin(2\pi f t)$, where t is the time. Effectively, this method models the system in a reference frame that moves up and down with the plenum chamber, distributor and fluidized bed as they vibrate up and down on the shaker.

2.3.2 Method 2: Vibrating a bottom plate represented by a horizontal layer of "frit particles"

This method was first proposed by Hartig et al. (2022). To implement this method, the movable flat surface is removed and the velocity of all particles in the virtual distributor is set to change with time following $v = 2\pi f A cos(2\pi f t)$. The gravitational acceleration is set as a constant of -9.81 m/s².

2.3.3 Method 3: Vibrating the bottom by using a movable flat surface

Inspired by Method 2, we propose to model the vibrated bottom by using a movable flat surface, which is smooth in nature. Like the position of the virtual distributor in Method 2, the flat

surface used in Method 3 (and Method 4 in the following) is located above the fixed bottom gas inlet boundary. Further, the flat surface is only seen by DEM and allows the gas phase to flow freely through it. As such, the problem of impacting an unrealistically bumpy plate by using "frit particles" in Method 2 is resolved. The method is implemented by (1) setting the velocity of all particles in the virtual distributor to change with time following $v = 2\pi f A \cos(2\pi f t)$ and (2) changing the position of the movable flat surface to follow $\delta = A \sin(2\pi f t)$. As such, the virtual distributor and movable flat surface can move synchronously, effectively avoiding numerical error caused by the movable flat surface penetrating into particles in the virtual distributor if they move asynchronously. The gravitational acceleration is set as a constant of -9.81 m/s².

2.3.4 Method 4: Proposed method

So far, the way to model the vibrated bottom has been improved in Method 3. However, the vibration of sidewalls in vibrated gas-fluidized beds is still not considered. With this in mind, standing on the basis of Method 3, we further propose to impose a tangential velocity on the walls to mimic the movement of sidewalls. As such, the vibration of both the bottom plate and sidewalls in a vibrated gas-fluidized bed can be well considered. Besides the steps (1) and (2) used in Method 3, one more step (3) imposing a tangential velocity $v = 2\pi f A cos(2\pi f t)$ on all sidewalls is necessary to implement Method 4. It should be stressed here again that even though the flat surface is moving in Methods 3 and 4, they differ from the moving mesh method, mainly in that the bottom gas inlet boundary is fixed and the CFD cells do not move over time in Methods 3 and 4. It is also worth noting that the motion of the walls and distributor are the same in Methods 1 and 4 with the difference that Method 1 is simulated in the moving (i.e. moving up and down with the shaker) reference frame and Method 4 is simulated in the stationary (i.e. staying stationary as the floor of the laboratory) reference frame. However, gas flow in Methods 1 and 4 may be different since the

size of the plenum chamber changes in Method 4 and the inlet gas velocity needed to model the gas flow in the plenum chamber in experiments is non-trivial for both the moving and stationary reference frames.

Table 2 summarizes the vibration modeling methods simulated in this paper.

Table 2. Summary of the vibration modeling methods used

Method	Gravity oscillated?	Distributor oscillated?	Virtual distributor used?	Flat plate on top of virtual distributor?	Side walls oscillated	Reference frame
Method 1	Yes	No	Yes	Yes	No	Moving
Method 2	No	Yes	Yes	No	No	Stationary
Method 3	No	Yes	Yes	Yes	No	Stationary
Method 4	No	Yes	Yes	Yes	Yes	Stationary

2.4 Modeling the gas inlet velocity condition

In the experiments, the gas enters the plenum chamber at a constant gas flow rate through two tubes (**Fig. 2b**). The tubes connect to a stationary mass flow controller and the plenum chamber which moves up and down with the shaker. The shaker has a wide base relative to the pseudo-2D fluidized bed, so it is unclear if the gas flow (i) stays constant in the stationary reference frame and thus oscillates in the moving reference frame or (ii) oscillates in the stationary reference frame, but is constant in the moving reference frame. Likely the flow in the plenum chamber is complex and neither (i) or (ii) fully captures the complex gas flow dynamics. Nevertheless, we seek to model these two potential gas flow possibilities. In the first series of simulations, to achieve a fair comparison of the vibration modeling methods as much as possible, the gas inlet boundary is specified as $U = 2\pi f A\cos(2\pi f t)$ for vibration modeling Method 1 to model the gas inlet velocity as constant in the stationary reference frame. For Methods 2-4, the gas inlet boundary is specified as a constant value of U = 0.30 m/s in the stationary reference frame, providing a direct comparison with Method 1 while also capturing the aspect of a constant gas flow rate coming from the mass

flow controller which is stationary in experiments. In the second series of simulations, the gas inlet velocity condition is set as U and $U + 2\pi f A cos(2\pi f t)$ for vibration modeling Method 1 and Method 4, respectively, to consider the possibility of vibrating the plenum chamber leading to the oscillation of gas flow rate in the plenum chamber. Here forward, we name these two additional simulations as Method 10 and Method 40, respectively. **Table 3** summarizes the two types of gas inlet possibilities and how they are modeled as gas inlet boundary conditions in the two specified two series of simulations. In all cases, the average gas inlet velocity is U = 0.30 m/s, equivalent to $1.4 U_{mf}$.

Table 3. Summary of gas inlet velocity conditions simulated

Simulation Series	Vibration Simulation Method	Gas Inlet Velocity in the Stationary Reference Frame	Gas Inlet Velocity in the Moving Reference Frame	Gas Inlet Velocity Specified in the Simulation	
Series 1	Method 1	Constant	Oscillating	$U - 2\pi f A cos(2\pi f t)$	
	Method 2	Constant	Oscillating	U	
	Method 3	Constant	Oscillating	U	
	Method 4	Constant	Oscillating	U	
Series 2	Method 1o	Oscillating	Constant	U	
	Method 4o	Oscillating	Oscillating	$U + 2\pi f A cos(2\pi f t)$	

2.5 Data post-processing

To compare the simulation results from different modeling methods for the vibration and the gas inlet velocity, the extent of the ordering in the predicted bubbling pattern was quantified by comparing the distributions of gas void fraction in the region of interest at two time instants separated by two vibration periods, 0.4 s, based on Pearson's correlation coefficient, *CC*. This method has been widely used in the field of tomography imaging to evaluate the similarity between two images (Guo et al., 2018). The definition of *CC* is:

$$CC = \frac{\sum_{i=1}^{N} (\varepsilon'_{g,i} - \overline{\varepsilon'_{g}})(\varepsilon_{g,i} - \overline{\varepsilon_{g}})}{\sqrt{\sum_{i=1}^{N} (\varepsilon'_{g,i} - \overline{\varepsilon'_{g}})^{2} \sum_{i=1}^{N} (\varepsilon_{g,i} - \overline{\varepsilon_{g}})^{2}}}$$
(12)

where N is the number of CFD cells in the region of interest, which is taken to cover the height from 64 mm to 126 mm, matching experiments, i is the cell index, $\varepsilon_{g,i}$ and $\varepsilon'_{g,i}$ are the gas void fraction averaged over the depth direction at cell i in the current time and in the time after two vibration periods, respectively, and $\overline{\varepsilon_g}$ and $\overline{\varepsilon_g'}$ are the average of $\varepsilon_{g,i}$ and $\varepsilon'_{g,i}$ over the region of interest, respectively. CC varies between 0 and 1 with a value of 1 for exact periodic repetition of structure and 0 for no periodic repetition. CC obtained across all the pair comparisons within the time between 2-8 s was calculated. Then, these data were divided into 3 segments, with each consisting of data from 2 s periods. Then, the averaged CC within each segment was obtained. The average and standard deviation of the averaged CC obtained in these 3 segments were then obtained and used to quantify the extent and stability of the structures, respectively, where the values of the standard deviation are shown as error bars.

Besides the extent of the structured bubbling pattern, bubble properties, including the bubble size and the horizontal bubble distance, were also compared for different modeling methods. The bubble properties were quantified based on digital image analysis of the distribution of gas void fraction averaged over the depth direction. At first, the images were binarized into bubble and particulate regions using a threshold of 0.8 for the void fraction, matching the value used in analyzing the grayscale images recorded in experiments (Guo et al., 2021), in which a threshold equaling 80% of the maximum pixel intensity from the recorded grayscale images was used. The bubble size was then determined as the diameter of a circle with the same area. The horizontal bubble distances were determined as the horizontal distances between the centers of two horizontally neighboring bubbles formed in the same row.

3. Results and discussion

3.1 Effects of varying vibration modeling methods

Figs. 3-7 show various time series of images for bubble dynamics over two vibration periods at vibration amplitudes of 1.0 mm (Fig. 3), 3.0 mm (Fig. 4), 4.5 mm (Fig. 5), 6.0 mm (Fig. 6) and 8.0 mm (Fig. 7) for (a) experiments and (b-e) CFD-DEM simulations from the first series of simulations (see Table 3) using (b) Method 1, (c) Method 2, (d) Method 3 and (e) Method 4 to model vibration. Here, instead of using physical time, the phase angle of vibration φ is used because it is a natural choice to show the dynamics of a repetitive pattern. The images shown in Figs. 3-7 are representative for the specified case, and for all cases, there is no significant difference between the views from the front side and the back side because the bed thickness is small. The initial particle height in Figs. 3-7 was 6.0 cm, the same in simulations and experiments. However, due to the limitation of the experimental setup and camera recording (Guo et al., 2023b), the bottom ~1.0 cm region cannot be recorded in experiments.

Experiments show that only A = 4.5 mm produces structured bubbling in which bubbles rise row by row without dynamic coalescing or splitting, and evenly sized bubbles are spaced regularly in rows with all bubbles aligned and bubble positions alternating each row. The number of bubbles in consecutive rows is repetitive between 3 and 4. The whole pattern repeats itself every two vibration periods, providing a robust "fingerprint" for the validation of simulations. Based on the evolving of force chains and particle circulation patterns from CFD-DEM simulations (Guo et al., 2021), it has been shown that the structured bubbling pattern forms as a result of rapid yet controlled transitions between solid-like and fluid-like behavior of particles around bubbles by vibration. The extent of structuring in experimental bubbling patterns at different vibration

amplitudes is quantified in **Fig. 8** with correlation coefficient showing a value above 0.8 in the A = 4.5 mm case and below 0.8 in all other cases. **Fig. 9** quantifies the bubble properties and level of structuring in the A = 4.5 mm case further showing (a) the average bubble size, (b) the standard deviation in bubble size, (c) the average bubble horizontal separation distance and (d) the standard deviation in bubble horizontal separation distance for experimental and all four simulation methods.

CFD-DEM simulations using Method 1 to model vibration predict the most ordered structuring of bubbles for the A = 1.0 mm case (Fig. 8), deviating sharply from experiments. Fairly structured bubbling is observed for the A = 4.5 mm case (Fig. 5), but bubbles form large horizontal bands at the distributor and form a lesser structured pattern high in the system than seen experimentally. Further, for the A = 4.5 mm case, the bubble size and horizontal bubble spacing as well as their standard deviations show large deviations as compared to experiments (Fig. 9). As mentioned in the introduction section, oscillating gravity was initially developed based on transforming the stationary reference frame to a moving coordinate system due to vibration (Acosta-Iborra et al., 2012; Jiang et al., 2020), which can be viewed as capturing the full physics of vibration. Therefore, one would expect Method 1 to give accurate predictions in cases with vibration. However, the deviations shown here demonstrate deficiencies in modeling vibration by oscillating gravity. Although we do not know why exactly Method 1 does not match experimental results well in this work, based on the comparison with other methods that will be presented in the following, our results indicate that modeling the fluidized bed in the stationary reference frame and modeling vibration directly and explicitly by applying the most accurate boundary conditions yields the best comparison with experimental results. In the next subsection, we investigate if different gas inlet velocity conditions can enable more accurate predictions using Method 1. We

leave further investigation on the exact reasons underlying the deficiencies of Method 1 in matching experimental results to future studies.

CFD-DEM simulations using Method 2 to model vibration predict the ordered structured bubbling for cases A = 4.5 mm, 6.0 mm and 8.0 mm with the most ordering at A = 6.0 mm (**Figs. 5-8**), deviating from experimental results. For the A = 4.5 mm case, the simulations with Method 2 predict bubble sizes much larger than those seen in experiments (**Fig. 9**), further showing issues with this method in capturing the dynamics of vibrated gas-fluidized beds with quantitative accuracy. These inaccuracies can be attributed to the sidewalls not moving as well as the bottom distributor being unrealistically bumpy.

CFD-DEM simulations using Method 3 to model vibration predict highly ordered structured bubbling for cases with A = 3.0 mm, 4.5 mm, 6.0 mm and 8.0 mm (Figs. 4-8), not matching the experimental results that structured bubbling only forms at A = 4.5 mm. For the A = 4.5 mm case, Method 3 predicts average bubble sizes and standard deviations in bubble size which are significantly larger than those observed experimentally (Fig. 9). These inaccuracies emphasize that in addition to the bottom distributor, it is important to capture the vibration of sidewalls, particularly for the pseudo-2D system that is thin in one direction as studied here, in order to capture the dynamics of vibrated gas-fluidized beds.

CFD-DEM simulations using Method 4 to model vibration predict the most structured bubbling dynamics at A = 4.5 mm with significantly lower structuring at other values of A, matching experimental results (**Figs. 3-8**). At A = 4.5 mm, both experiments and Method 4 show rows of 3 or 4 bubbles spanning the system, further emphasizing the accuracy of this method. Method 4 matches the average bubble size for the experimental A = 4.5 mm case most accurately of all four methods (**Fig. 9**). Further, Method 4 also matches the experimental values of average

horizontal distance between bubbles and the standard deviations in bubble size and horizontal spacing fairly well (**Fig. 9**). These results emphasize that matching the physics of vibrating a gasfluidized bed most accurately in the simulation method by modeling the distributor as fairly flat and moving up and down as well as modeling the sidewalls as moving up and down is key to matching experimental results accurately. The predictions of Method 4 do not match experimental results exactly, notably predicting more ordering in bubbling at A = 1.0 mm and 8.0 mm than seen experimentally (**Fig. 8**). Nonetheless, the significant increase in accuracy of the proposed Method 4 for modeling bubble dynamics in vibrated gas-fluidized beds as compared to the other methods provides strong reasoning for using this proposed method to model vibration in future work.

It should be noted that in Figure 9, a threshold of 0.8 for the void fraction is used to identify bubbles in simulations. Two additional threshold values of 0.7 and 0.9 were also tested in simulations, which lie in the value range normally used in the literature (Guo et al., 2018). Supporting Information Figure S2 compares the predicted bubble properties in simulations from different vibration modeling methods and based on different values for the threshold with experiments. As can be seen, using different values for the threshold can affect the measured bubble size but has no significant effect on the horizontal distance between bubbles. Overall, the use of different values for the threshold does not affect the relative accuracy of different vibration modeling methods in the prediction of bubble properties. Nevertheless, it should be stressed that evaluating different methods based on the statistically averaged bubble properties might give the wrong conclusion. For model validation, the statistically averaged bubble properties must be considered together with the bubbling pattern, highlighting the role of structured bubbling pattern as a robust "fingerprint" for this aim.

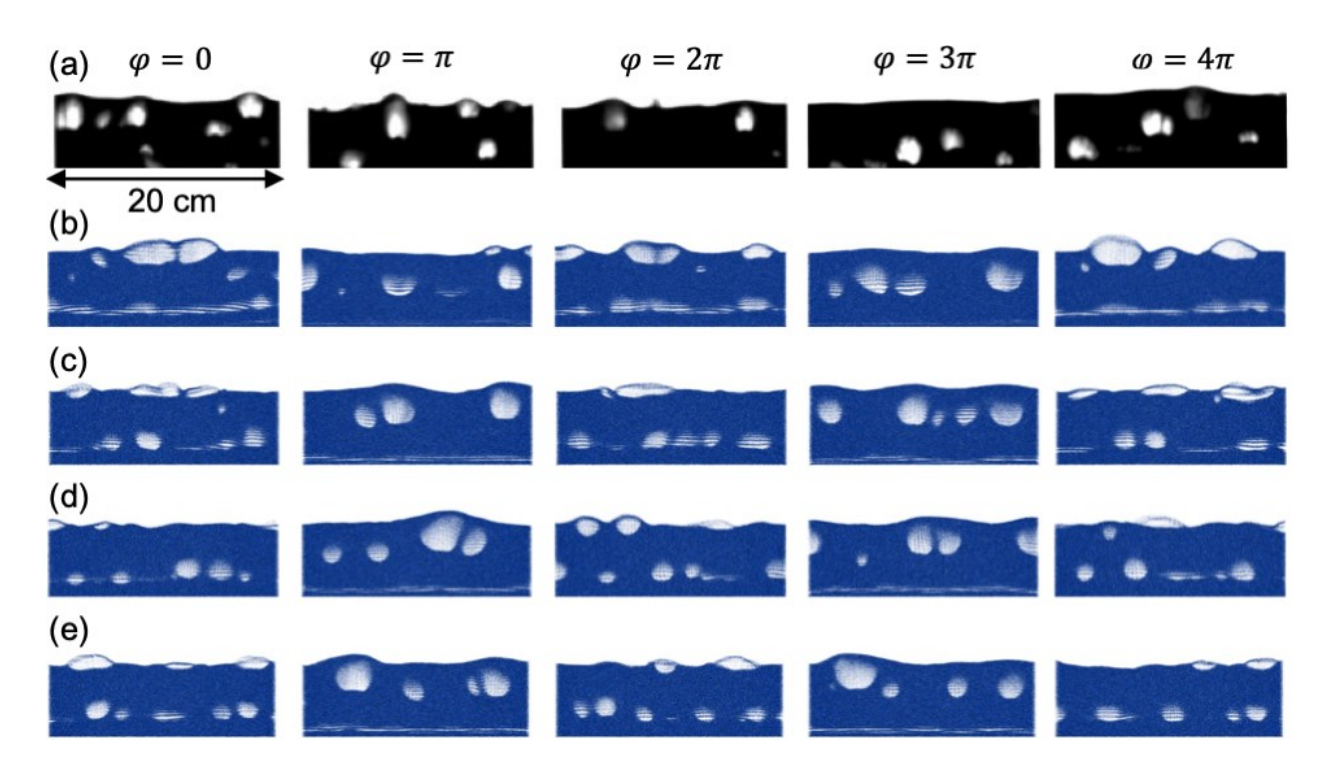


Figure 3. Time series images of the bubbling patterns at the vibration amplitude of 1.0 mm from (a) experiments and (b-e) CFD-DEM simulations using (b) Method 1, (c) Method 2, (d) Method 3 and (e) Method 4 to model vibration. Other conditions: vibration frequency: 5 Hz and gas flow rate: see **Table 3**.

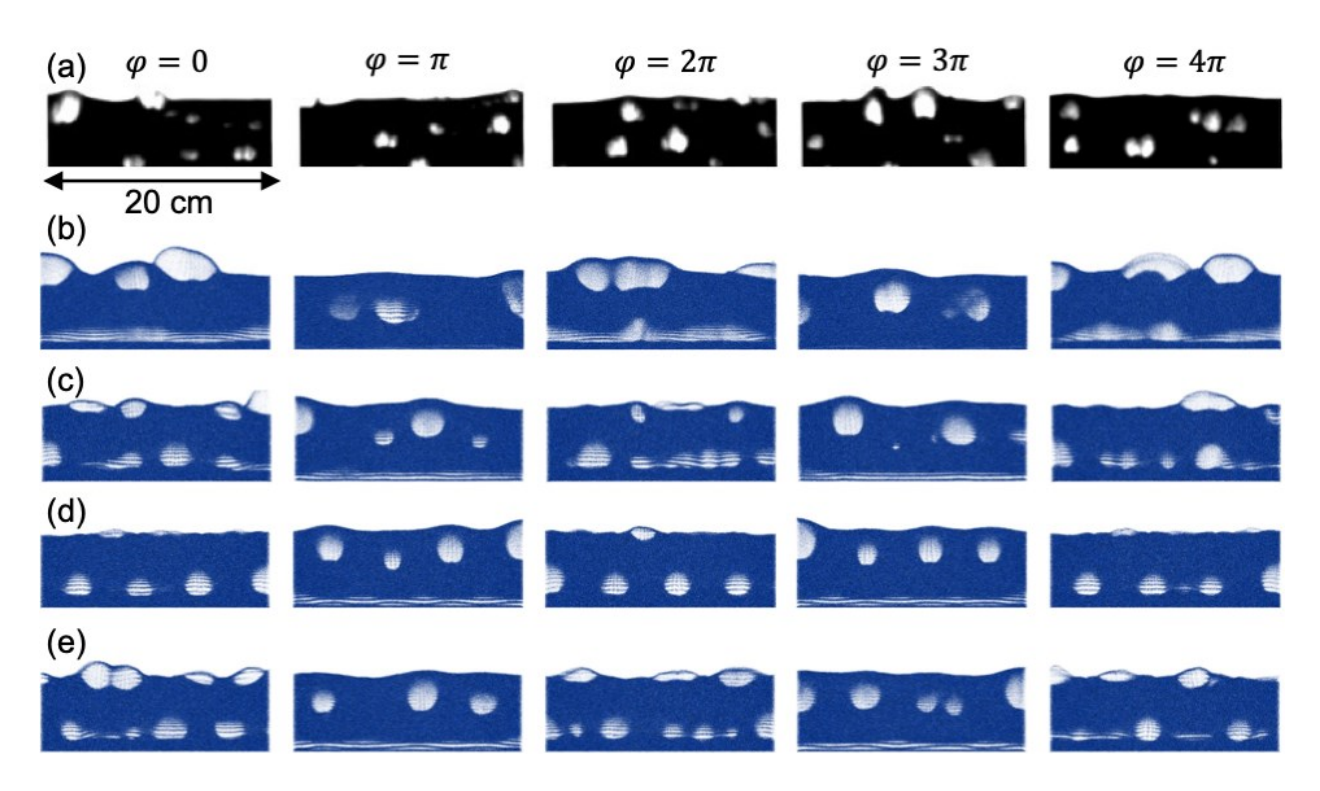


Figure 4. Time series images of the bubbling patterns at the vibration amplitude of 3.0 mm from (a) experiments and (b-e) CFD-DEM simulations using (b) Method 1, (c) Method 2, (d) Method 3 and (e) Method 4 to model vibration. Other conditions: vibration frequency: 5 Hz and gas flow rate: see **Table 3**.

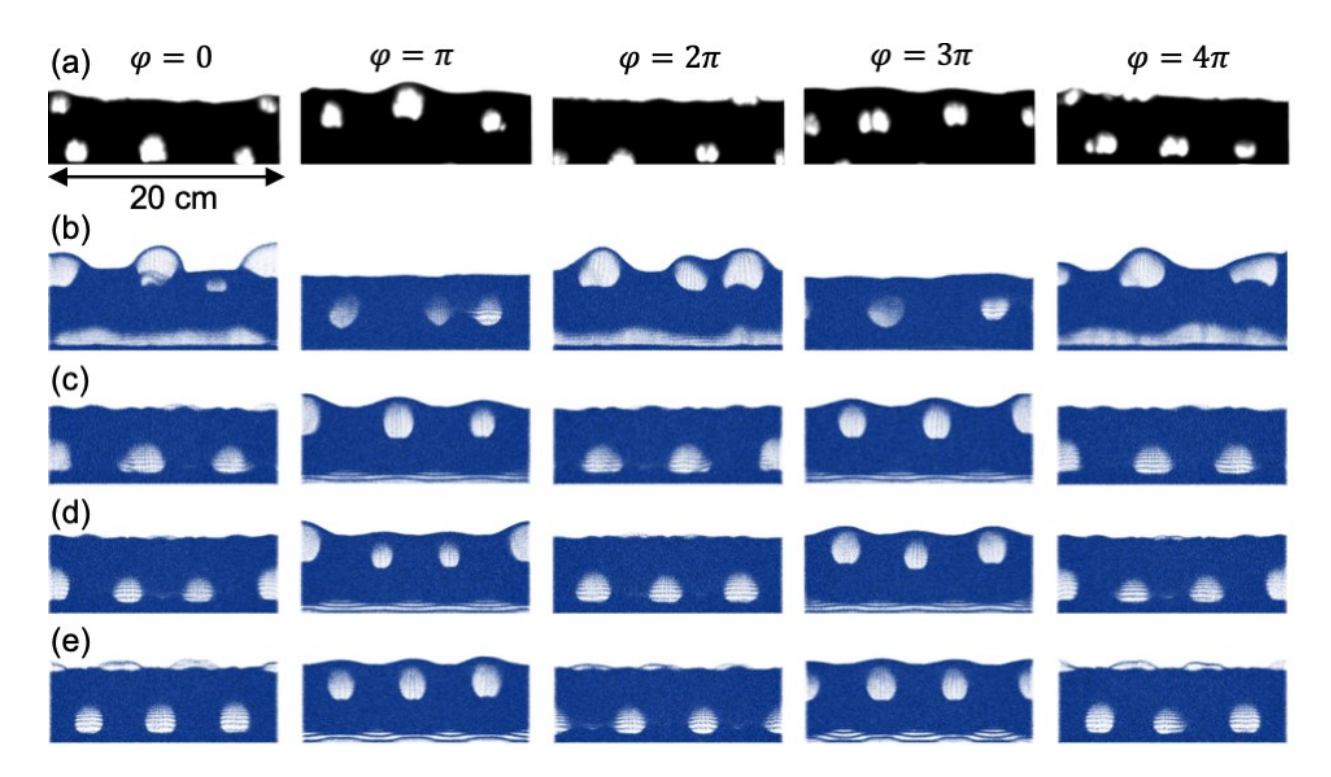


Figure 5. Time series images of the bubbling patterns at the vibration amplitude of 4.5 mm from (a) experiments and (b-e) CFD-DEM simulations using (b) Method 1, (c) Method 2, (d) Method 3 and (e) Method 4 to model vibration. Other conditions: vibration frequency: 5 Hz and gas flow rate: see **Table 3**.

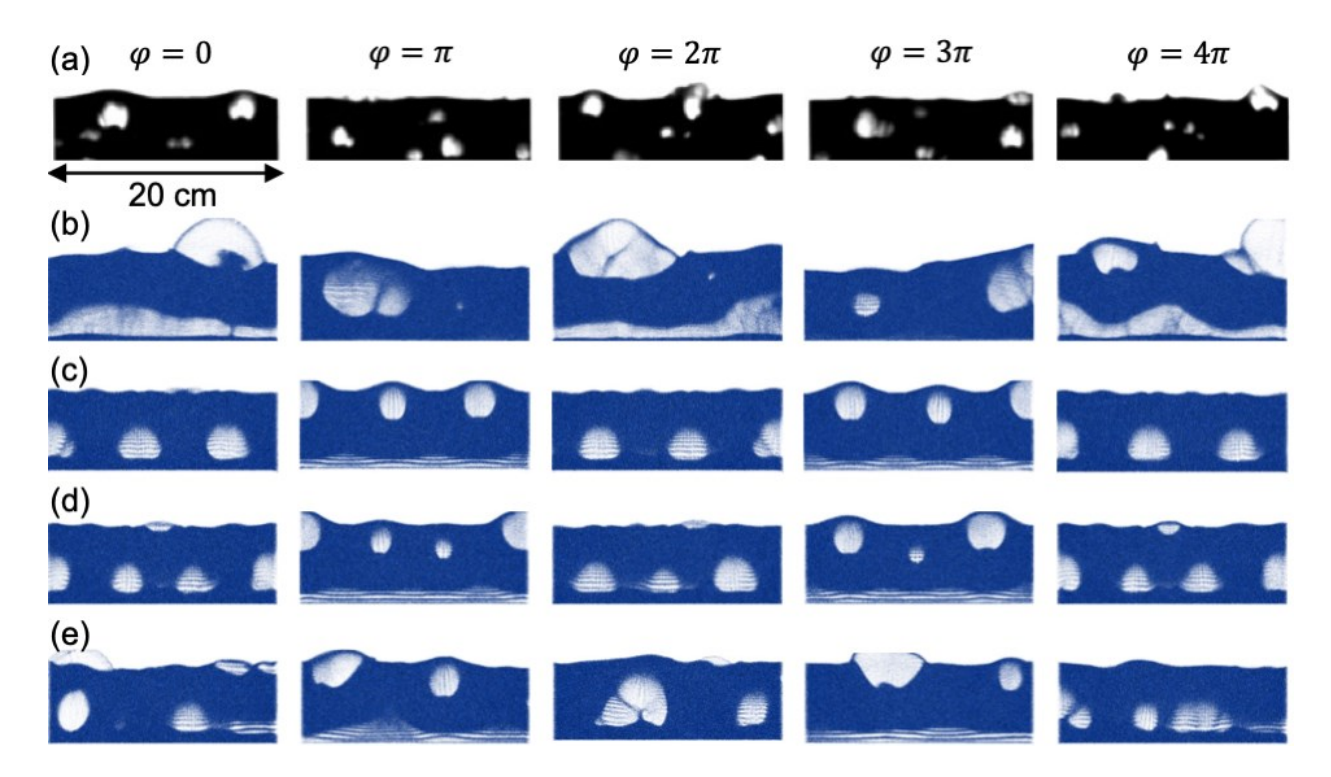


Figure 6. Time series images of the bubbling patterns at the vibration amplitude of 6.0 mm from (a) experiments and (b-e) CFD-DEM simulations using (b) Method 1, (c) Method 2, (d) Method 3 and (e) Method 4 to model vibration. Other conditions: vibration frequency: 5 Hz and gas flow rate: see **Table 3**.

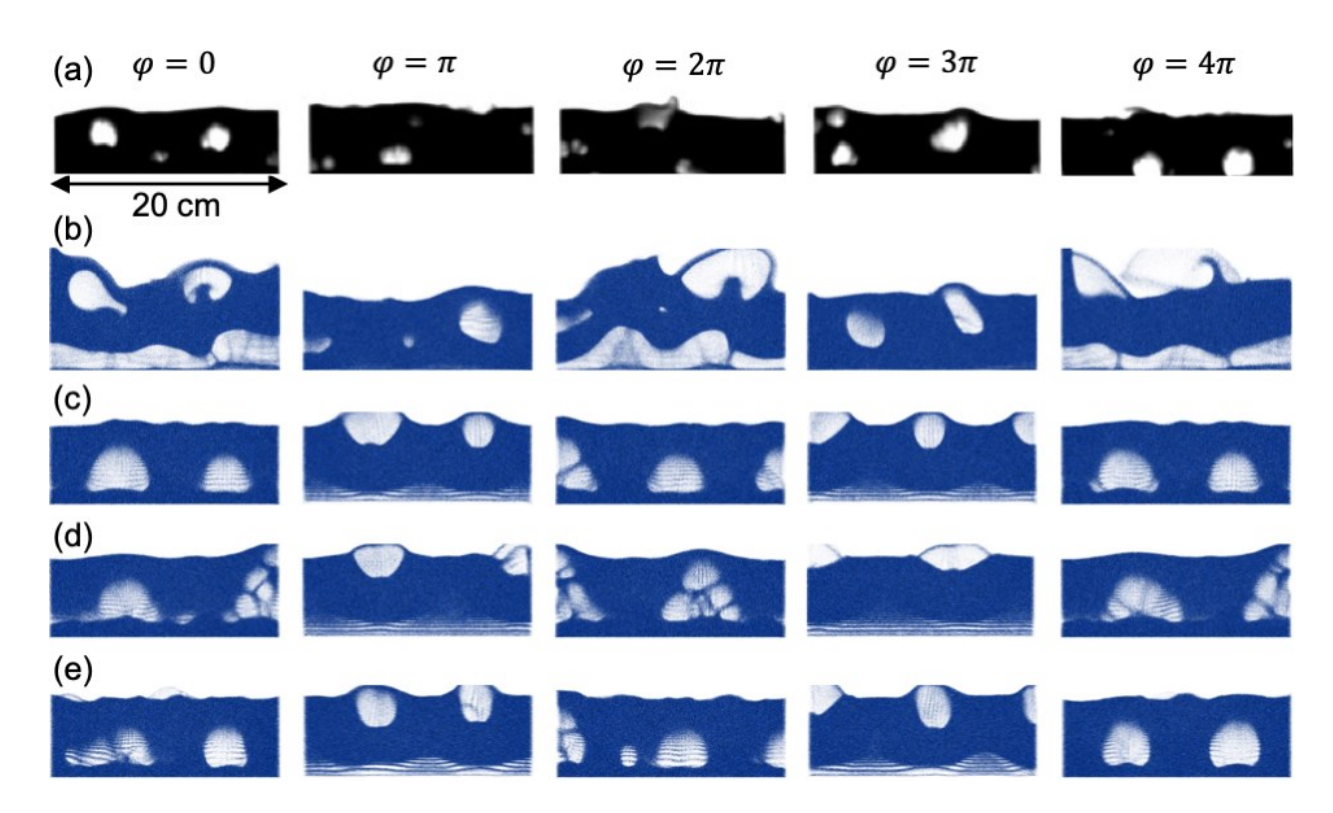


Figure 7. Time series images of the bubbling patterns at the vibration amplitude of 8.0 mm from (a) experiments and (b-e) CFD-DEM simulations using (b) Method 1, (c) Method 2, (d) Method 3 and (e) Method 4 to model vibration. Other conditions: vibration frequency: 5 Hz and gas flow rate: see **Table 3**.

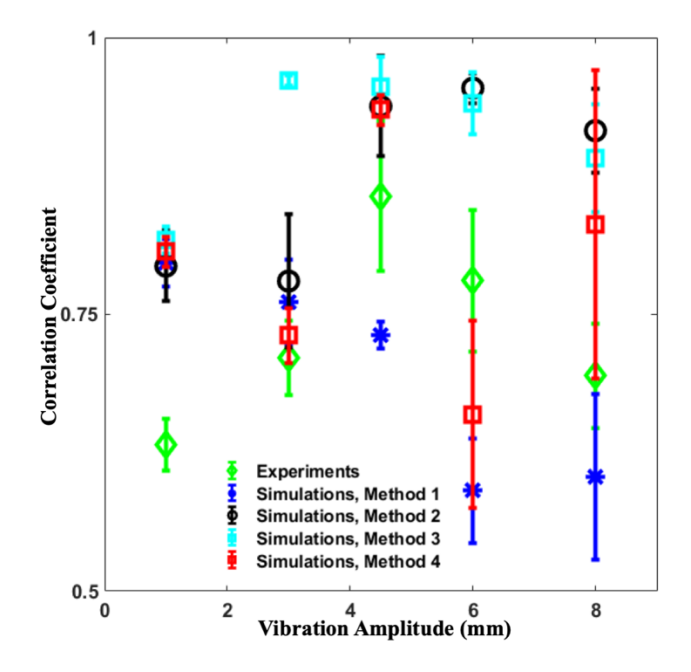


Figure 8. Quantification of the extent and stability of the bubbling structures obtained from experiments and CFD-DEM simulations by different vibration modeling methods and at different vibration amplitudes. Other conditions: vibration frequency: 5 Hz and gas flow rate: see **Table 3**.

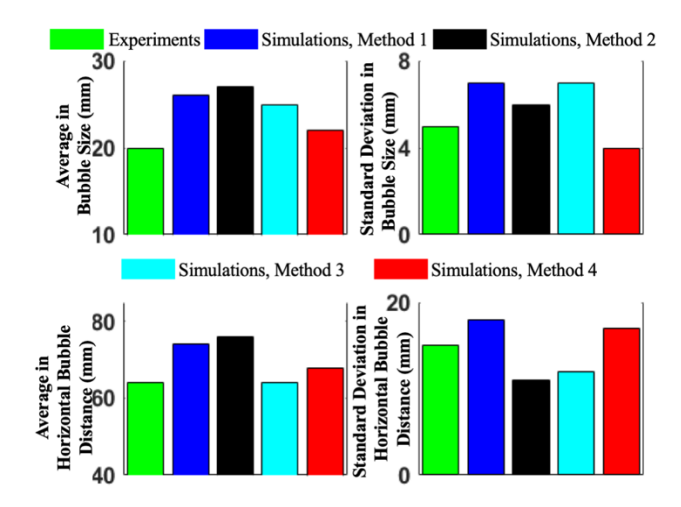


Figure 9. Comparison of the predicted bubble properties from different vibration modeling methods with experiments. The vibration amplitude used here is 4.5 mm. Other conditions: vibration frequency: 5 Hz and gas flow rate: see **Table 3**.

Fig. 10 compares the total wall time taken to run simulations for 8 s for different vibration modeling methods and at different vibration amplitudes with simulations running in the distributed memory parallel scheme (Garg et al., 2012) on 24 processors. A longer wall time indicates a higher computational cost. Generally, the required wall time increases with the increase of vibration amplitude for all the methods because the effects of vibration become more computationally expensive likely due to increased particle collisions at larger vibration amplitudes. Almost at all the tested vibration amplitudes, the required wall time by Method 1 is the shortest, followed by Method 2, and then by Method 3, and finally by Method 4. The increased computational expense can be attributed to the increased complexity in moving from Method 1 to Method 4 in terms of added numerical calculations which must be added to account for the more realistic physics of vibrating a gas-fluidized bed. Nevertheless, the difference in the required wall time is not significant between different methods: the total wall time of Method 4 is only 9.3% more than that of Method 1 on average. Yet as shown previously, Method 4 predicts the vibration amplitude at which structured bubbling is formed and which it is not formed, while other methods cannot.

Further, the properties of bubble size and distance between bubbles are predicted somewhat better by Method 4, although not conclusively better than other methods. Considering these results, we suggest Method 4 as the best method for modeling vibrated gas-fluidized beds. We leave it to future studies of other regimes of vibrated gas-fluidized beds in experiments and simulations to further test this assertion.

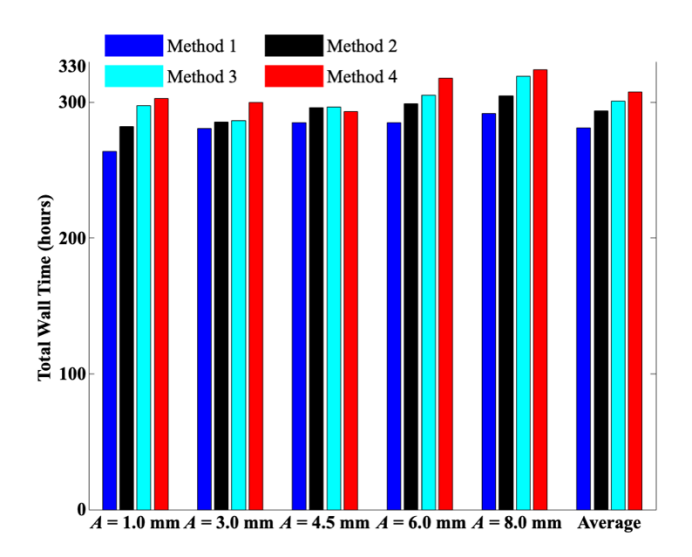


Figure 10. Total wall time taken to run simulations for 8 s for different vibration modeling methods and at different vibration amplitudes with simulations running in parallel on 24 processors.

Without loss of generality, an additional simulation was performed using Method 4 with all settings the same as the cases shown above but with a vibration amplitude of 0 mm. As such, vibration is turned off and the bed can be treated as operating at the freely bubbling regime. Supporting Information Figure S3 compares the typical bubbling pattern predicted from simulations to that obtained from experiments at the same superficial gas velocity, $1.4U_{mf}$. Clearly, simulations agree well with experiments, showing that many bubbles with different sizes and shapes rising in a chaotic manner in the bed. The predicted bubble size from simulations also matches quantitatively with experiments: the average bubble size obtained from simulations and experiments is 7.8 ± 2.9 mm and 8.5 ± 3.8 mm, respectively. Therefore, the proposed vibration modeling method can also work in cases with vibration turned off.

3.2 Effects of varying gas inlet boundary conditions

Fig. 11 quantifies the effects of the gas inlet velocity conditions and vibration amplitude used for different vibration modeling methods from the second series of simulations (see Table 3) on the repetition of bubble patterns across two vibration periods as quantified through the correlation coefficient. Results show that all methods erroneously overestimate the correlation coefficient in the 1.0 mm amplitude case, and the difference between the accuracy of the methods lie in the higher amplitude cases. Only Method 4 captures the highest correlation coefficient maximized at 4.5 mm amplitude, indicating this method with walls moving and gas velocity and gravity constant captures a key experimental result which other methods do not. Significant quantitative differences between Methods 1, 10, 4 and 40 indicate that while Methods 1 and 4 and Methods 4 and 40 respectively seem close to just being a change in reference frame, specific details of gas entry into the fluidized bed through the distributor which differ in these methods are important for modeling.

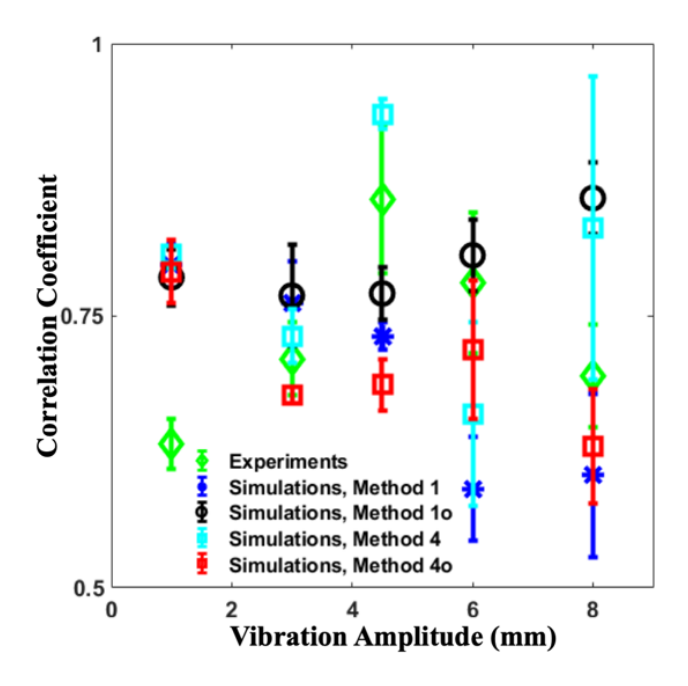


Figure 11. Quantification of the extent and stability of the bubbling structures obtained from experiments and CFD-DEM simulations by different modeling methods of vibration and gas inlet

conditions (see **Table 3**) and at different vibration amplitudes. Other conditions: vibration frequency: 5 Hz.

Fig. 12 shows the effects of changing gas inlet velocity boundary conditions (see Table 3) on bubble dynamics produced over two vibration cycles for the experimental case with the most structured bubbling. Fig. 13 quantifies these effects on bubble size and spacing between bubbles. Results show that Method 4 predicts the most ordered and repeating bubble structure, matching experiments. Other methods also show a certain degree of structuring in bubbles, but the structuring is significantly less than that seen qualitatively and quantitatively in experiments.

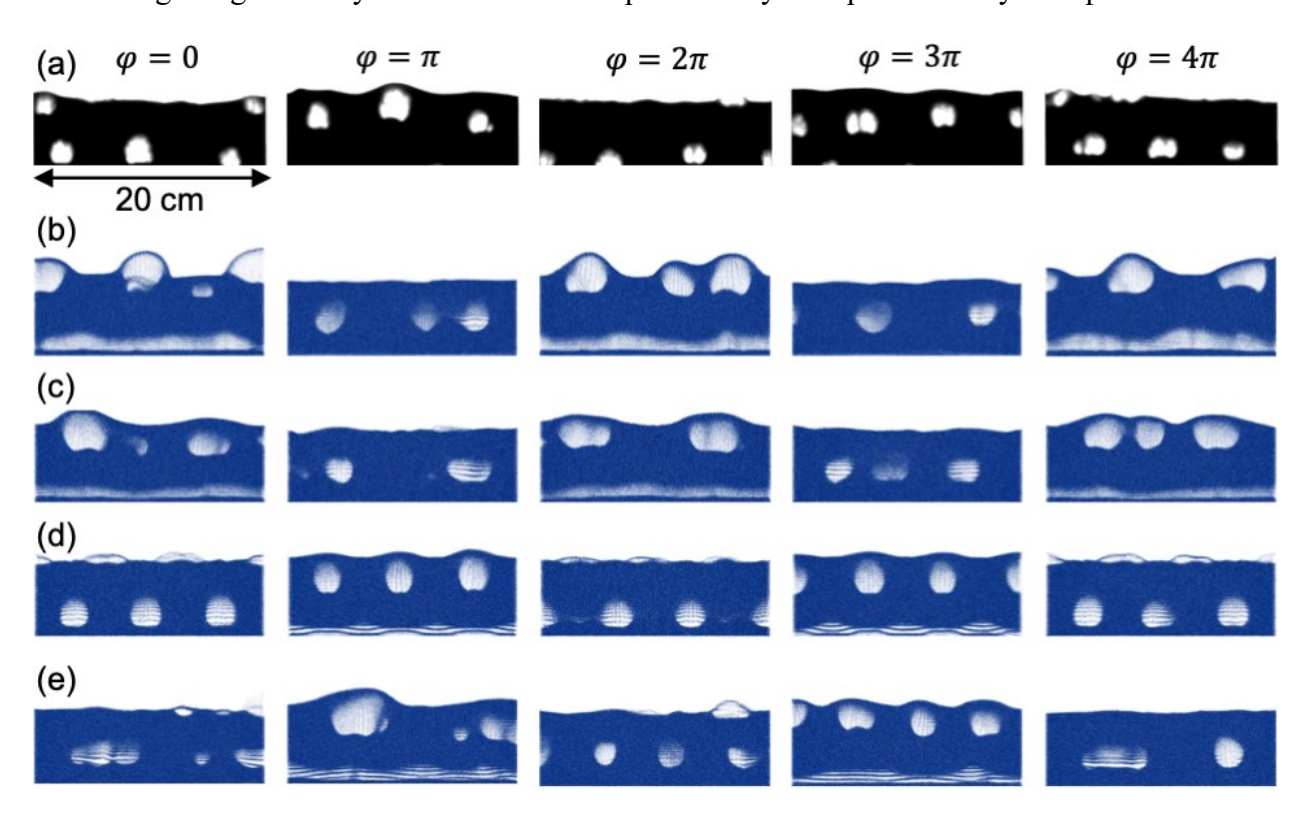


Figure 12. Time series images of the bubbling patterns at the vibration amplitude of 4.5 mm from (a) experiments and (b-e) CFD-DEM simulations using (b) Method 1, (c) Method 10, (d) Method 4 and (e) Method 40 to model vibration and gas inlet conditions (see **Table 3**). Other conditions: vibration frequency: 5 Hz.

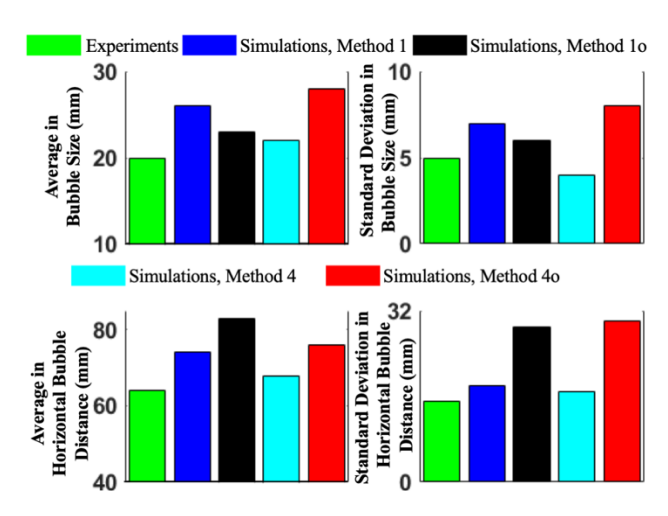


Figure 13. Comparison of the predicted bubble properties from simulations with different modeling methods of vibration and gas inlet velocity (see **Table 3**) with experiments. The vibration amplitude used here is 4.5 mm. Other conditions: vibration frequency: 5 Hz.

Fig. 13 shows the effects of gas inlet velocity modeling on bubble size and spacing for the 4.5 mm amplitude case in which structured bubbling is observed experimentally. Results show that Method 4 matches experimental results most accurately across the various bubbling characteristics, again emphasizing the superior accuracy in this method capturing the physics of the experimental system.

Fig. 14 shows the effects of varying the gas inlet velocity over the course of two vibration cycles on the gas flow in the plenum, distributor and lower part of the fluidized bed for the 4.5 mm amplitude case in the stationary reference frame. Results show that Method 4, which matches experimental results for bubbling dynamics most accurately, involves a relatively constant gas flow through the plenum chamber due to the constant gas inlet velocity, yet a highly variable gas flow through the distributor, since the distributor moves up and down. At the top of the distributor and just above the distributor, gas channels into bubbles which are forming or have just formed at regularly spaced horizontal positions, generating the structured bubbling. Method 1 has a similar constant gas velocity in the plenum chamber and oscillating velocity through the distributor, reflecting the fact that Methods 1 and 4 are nearly a complete reference frame transformation of

one another. However, the same structuring of diagonal gas flow at the top of the distributor to form regularly spaced bubbles is not observed in Method 1. The differences between Methods 1 and 4 can be attributed to differences in the accelerations of the gas in the plenum chamber and the distributor as well as the volume of the distributor (constant in Method 1, but varying in Method 4) due to particulars of the boundary conditions and modeling of the distributor motion. While there is no clear way to know whether Method 1 or Method 4 would match the experimental system better a priori, the results here demonstrate that Method 4 captures the structured bubbling dynamics more accurately than Method 1. Methods 10 and 40 have varying gas velocity in both the plenum chamber and the distributor due to the oscillating inlet gas velocity. Notably, the oscillating gas inlet velocity in Methods 10 and 40 leads to gas velocity through the distributor which is out-of-phase with that seen in the constant gas inlet velocity cases of Methods 1 and 4. Diagonal gas velocity vectors are also observed at the top of the distributor and the bottom of the bed in Methods 10 and 40, indicating channeling to form bubbles, yet the same regular horizontal spacing of bubbles observed in Method 4 is not observed in Methods 10 and 40. These results indicate that gas flow in the experimental system is better modeled here by gas flow being constant in time in the stationary reference frame, rather than oscillating in time.

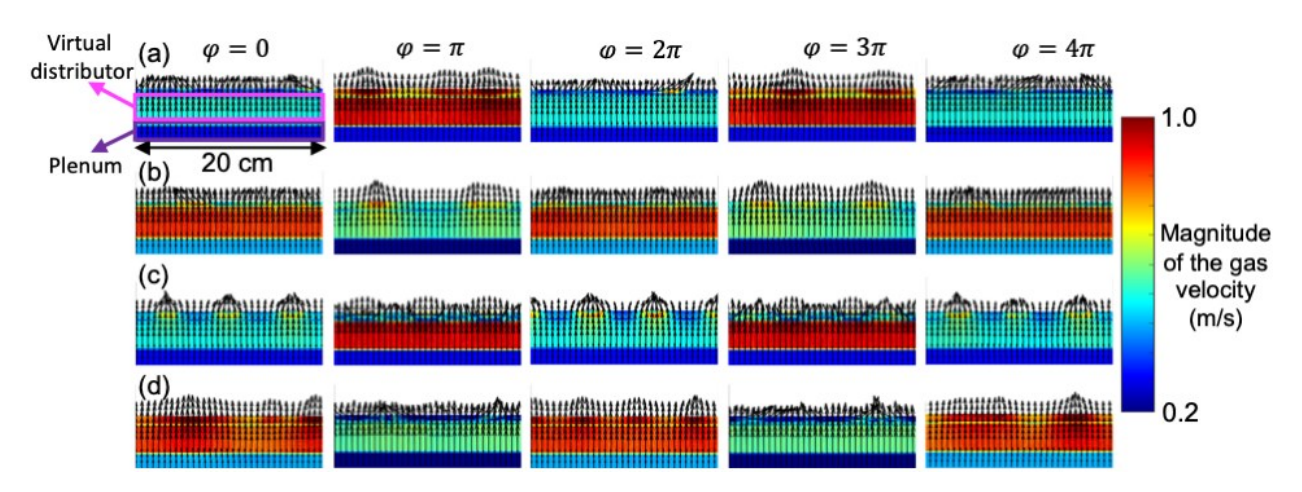


Figure 14. Distribution of gas velocities in the virtual plenum, distributor and just above the distributor over the course of two vibration cycles for the simulation cases shown in **Figure 12**. The gas inlet velocity and vibration are modeled by (a) Method 1, (b) Method 10, (c) Method 4 and (d) Method 40. The color indicates the magnitude of the gas velocity and the arrows indicates the gas flow vector. All results are shown in the stationary reference frame.

4. Conclusion

This paper compares (i) methods for modeling vibration and (ii) methods for modeling inlet gas velocity in CFD-DEM simulations of vibrated gas-fluidized beds. Simulation predictions of bubble dynamics are compared with those from experiments under vibration conditions in which structured bubbling can be observed because structured bubbling dynamics are deterministic and repeat themselves periodically, avoiding the need for comparison over statistically averaged chaotic dynamics.

The methods for modeling vibration are: Method 1 by oscillating gravity to model the system in the moving reference frame, Method 2 by vibrating a bottom plate represented by a horizontal layer of "frit particles", Method 3 by vibrating the bottom using a movable flat surface that is located above the bottom gas inlet boundary and only seen by DEM, and Method 4 by standing on the basis of Method 3 and also imposing a tangential velocity on the sidewalls. Results show that modeling vibration as an oscillating gravity force in Method 1 does not determine optimal vibration conditions for producing structure, although it was developed based on the transformation of coordinate system, which should capture the full physics of vibration. To further investigate this result, we tested the effect of different gas inlet conditions in different coordinate system shifts as described below. Models 2 and 3 which model vibration via movement of the distributor in the stationary reference frame achieve a higher level of accuracy in some cases based

on comparison with experiments, yet these methods do not model the motion of sidewalls, leading to predictions of structured bubbling under vibration conditions which do not produce structured bubbling in experiments. The proposed Method 4 accounts for both motion of the bottom plate and the sidewalls and predicts structured bubbling only under the same conditions observed experimentally while also predicting the bubble size most accurately of all the methods tested. Further, the proposed Method 4 is only slightly more computationally expensive than the other three methods and can work well in cases with vibration turned off. As such, we view this proposed method as the most accurate method to be used for future simulations of vibrated gas-fluidized beds without the computational expense of using a moving mesh.

A further aspect investigated in this study was the gas inlet conditions which best capture the physics of a vibrated gas-fluidized bed in the case of an experimental system with a constant gas flow rate and a plenum chamber, distributor and fluidized bed which are all vibrated together. Under such circumstances, it is non-trivial what gas flow conditions occur within the plenum chamber, distributor and entry to the fluidized bed, and how these are best represented in the stationary and moving reference frames. As such, four methods were investigated: Methods 1 and 4 in the moving and stationary reference frames, respectively, with a constant gas inlet velocity into the plenum chamber in the stationary reference frame, as well as Methods 10 and 40 in the moving and stationary reference frames, respectively, with an oscillating gas inlet velocity into the plenum chamber in the stationary reference frame. It was determined that the constant gas inlet velocity into the plenum chamber simulations performed more accurately than those with oscillating gas inlet velocity into the plenum chamber in the stationary reference frame. Further, small subtleties in the gas flow in the plenum chamber and the distributor between Methods 1 and 4 made the two simulations not a simple transformation of coordinate and had a strong impact on

the ultimate bubble dynamics in the system. Results showed that Method 4 in the stationary reference frame provided the most accurate modeling of the deterministic structured bubbling dynamics. As such, this paper indicates that modeling a vibrated gas-fluidized bed in which the entire plenum chamber and bed is vibrated and gas flow is held constant is best modeled using a moving distributor and walls in the stationary reference frame with a constant gas inlet velocity (referred to as Method 4 in this paper).

Acknowledgement

This work was financially supported by Office of Naval Research grant N00014-23-1-2041 and National Science Foundation grant 2144763. We acknowledge computing resources from Columbia University's Shared Research Computing Facility project and National Science Foundation's Advanced Cyberinfrastructure Coordination Ecosystem: Services & Support (ACCESS) program.

References

- Acosta-Iborra, A., Hernández-Jiménez, F., de Vega, M., Briongos, J.V., 2012. A novel methodology for simulating vibrated fluidized beds using two-fluid models. Chemical Engineering Journal 198–199, 261–274. https://doi.org/10.1016/j.cej.2012.05.098
- Cano-Pleite, E., Hernández-Jiménez, F., Acosta-Iborra, A., 2015. Compressible-gas two-fluid modeling of isolated bubbles in a vertically vibrated fluidized bed and comparison with experiments. Chemical Engineering Journal 271, 287–299. https://doi.org/10.1016/j.cej.2015.02.096
- Chew, J.W., LaMarche, W.C.Q., Cocco, R.A., 2022. 100 years of scaling up fluidized bed and circulating fluidized bed reactors. Powder Technology 409, 117813. https://doi.org/10.1016/j.powtec.2022.117813
- Ding, J., Gidaspow, D., 1990. A bubbling fluidization model using kinetic theory of granular flow. AIChE Journal 36, 523–538. https://doi.org/10.1002/aic.690360404
- Doustdar, M.M., Kazemi, H., 2019. Effects of fixed and dynamic mesh methods on simulation of stepped planing craft. Journal of Ocean Engineering and Science 4, 33–48. https://doi.org/10.1016/j.joes.2018.12.005
- El-Emam, M.A., Zhou, L., Shi, W., Han, C., Bai, L., Agarwal, R., 2021. Theories and Applications of CFD–DEM Coupling Approach for Granular Flow: A Review. Arch Computat Methods Eng 28, 4979–5020. https://doi.org/10.1007/s11831-021-09568-9

- Garg, R., Galvin, J., Li, T., Pannala, S., 2012. Open-source MFIX-DEM software for gas—solids flows: Part I—Verification studies. Powder Technology, Selected Papers from the 2010 NETL Multiphase Flow Workshop 220, 122–137. https://doi.org/10.1016/j.powtec.2011.09.019
- Geldart, D., 1973. Types of gas fluidization. Powder Technology 7, 285–292. https://doi.org/10.1016/0032-5910(73)80037-3
- Grace, J.R., Bi, X., Ellis, N., 2020. Essentials of Fluidization Technology. John Wiley & Sons.
- Guo, Q., Boyce, C.M., 2022. Structured bubbling in layered gas-fluidized beds subject to vibration: A CFD-DEM study. AIChE Journal 68, e17709. https://doi.org/10.1002/aic.17709
- Guo, Q., Chiu, S., Da, W., Boyce, C.M., 2023a. Heat transfer within dynamically structured bubbling fluidized beds subject to vibration: A two-fluid modeling study. AIChE Journal 69, e17970. https://doi.org/10.1002/aic.17970
- Guo, Q., Da, W., Wu, R., Zhang, Y., Wei, J., Boyce, C.M., 2023b. Faraday wave instability analog in vibrated gas-fluidized granular particles. Phys. Rev. E 107, 034603. https://doi.org/10.1103/PhysRevE.107.034603
- Guo, Q., Meng, S., Wang, D., Zhao, Y., Ye, M., Yang, W., Liu, Z., 2018. Investigation of gassolid bubbling fluidized beds using ECT with a modified Tikhonov regularization technique. AIChE Journal 64, 29–41. https://doi.org/10.1002/aic.15879
- Guo, Q., Spitler, C., Sanghishetty, J.M., Boyce, C.M., 2023c. Advances in vibrated gas-fluidized beds. Current Opinion in Chemical Engineering 42, 100977. https://doi.org/10.1016/j.coche.2023.100977
- Guo, Q., Zhang, Y., Kovar, T.M., Xi, K., Boyce, C.M., 2022a. A Rayleigh–Bénard convection instability analog in vibrated gas-fluidized granular particles. Soft Matter 18, 3323–3327. https://doi.org/10.1039/D1SM01803E
- Guo, Q., Zhang, Y., Padash, A., Xi, K., Kovar, T.M., Boyce, C.M., 2021. Dynamically structured bubbling in vibrated gas-fluidized granular materials. Proceedings of the National Academy of Sciences 118, e2108647118. https://doi.org/10.1073/pnas.2108647118
- Guo, Q., Zhang, Y., Vazquez, C., Xi, K., Boyce, C.M., 2022b. Multifluid model simulations of gravitational instabilities in fluidized binary granular materials. AIChE Journal 68, e17714. https://doi.org/10.1002/aic.17714
- Hartig, J., Howard, H.C., Stelmach, T.J., Weimer, A.W., 2021. DEM modeling of fine powder convection in a continuous vibrating bed reactor. Powder Technology 386, 209–220. https://doi.org/10.1016/j.powtec.2021.03.038
- Hartig, J., Shetty, A., Conklin, D.R., Weimer, A.W., 2022. Aeration and cohesive effects on flowability in a vibrating powder conveyor. Powder Technology 408, 117724. https://doi.org/10.1016/j.powtec.2022.117724
- Hoorijani, H., Zarghami, R., Nosrati, K., Mostoufi, N., 2021. Investigating the hydrodynamics of vibro-fluidized bed of hydrophilic titanium nanoparticles. Chemical Engineering Research and Design 174, 486–497. https://doi.org/10.1016/j.cherd.2021.08.026
- Jiang, Z., Rai, K., Tsuji, T., Washino, K., Tanaka, T., Oshitani, J., 2020. Upscaled DEM-CFD model for vibrated fluidized bed based on particle-scale similarities. Advanced Powder Technology 31, 4598–4618. https://doi.org/10.1016/j.apt.2020.10.009
- Jurtz, N., Kruggel-Emden, H., Baran, O., Aglave, R., Cocco, R., Kraume, M., 2020. Impact of Contact Scaling and Drag Calculation on the Accuracy of Coarse-Grained Discrete

- Element Method. Chemical Engineering & Technology 43, 1959–1970. https://doi.org/10.1002/ceat.202000055
- Lehmann, S.E., Hartge, E.-U., Jongsma, A., deLeeuw, I.-M., Innings, F., Heinrich, S., 2019. Fluidization characteristics of cohesive powders in vibrated fluidized bed drying at low vibration frequencies. Powder Technology 357, 54–63. https://doi.org/10.1016/j.powtec.2019.08.105
- Li, Z., Xiang, J., Liu, X., Li, X., Li, L., Shan, B., Chen, R., 2022. A combined multiscale modeling and experimental study on surface modification of high-volume micronanoparticles with atomic accuracy. Int. J. Extrem. Manuf. 4, 025101. https://doi.org/10.1088/2631-7990/ac529c
- McLaren, C.P., Kovar, T.M., Penn, A., Muller, C.R., Boyce, C.M., 2019. Gravitational instabilities in binary granular materials. Proceedings of the National Academy of Sciences 116, 9263–9268. https://doi.org/10.1073/pnas.1820820116
- Noda, K., Mawatari, Y., Uchida, S., 1998. Flow patterns of fine particles in a vibrated fluidized bed under atmospheric or reduced pressure. Powder Technology 99, 11–14. https://doi.org/10.1016/S0032-5910(98)00079-5
- Omidi, J., Punch, O.J., Guo, Q., Boyce, C.M., 2024. Faraday waves in gas-fluidized beds subject to combined vertical and horizontal vibration. Powder Technology 438, 119648. https://doi.org/10.1016/j.powtec.2024.119648
- Peng, Z., Doroodchi, E., Luo, C., Moghtaderi, B., 2014. Influence of void fraction calculation on fidelity of CFD-DEM simulation of gas-solid bubbling fluidized beds. AIChE Journal 60, 2000–2018. https://doi.org/10.1002/aic.14421
- Rahimi, M.R., Azizi, N., Hosseini, S.H., Ahmadi, G., 2013. CFD study of hydrodynamics behavior of a vibrating fluidized bed using kinetic-frictional stress model of granular flow. Korean J. Chem. Eng. 30, 761–770. https://doi.org/10.1007/s11814-012-0200-3
- Tatemoto, Y., Mawatari, Y., Noda, K., 2005. Numerical simulation of cohesive particle motion in vibrated fluidized bed. Chemical Engineering Science 60, 5010–5021. https://doi.org/10.1016/j.ces.2005.03.058
- Tatemoto, Y., Mawatari, Y., Yasukawa, T., Noda, K., 2004. Numerical simulation of particle motion in vibrated fluidized bed. Chemical Engineering Science 59, 437–447. https://doi.org/10.1016/j.ces.2003.10.005
- Tsuji, Y., Tanaka, T., Ishida, T., 1992. Lagrangian numerical simulation of plug flow of cohesionless particles in a horizontal pipe. Powder Technology 71, 239–250. https://doi.org/10.1016/0032-5910(92)88030-L
- Valverde, J.M., Castellanos, A., Sanchez Quintanilla, M.A., 2001. Self-Diffusion in a Gas-Fluidized Bed of Fine Powder. Phys. Rev. Lett. 86, 3020–3023. https://doi.org/10.1103/PhysRevLett.86.3020
- van der Hoef, M.A., Ye, M., van Sint Annaland, M., Andrews, A.T., Sundaresan, S., Kuipers, J.A.M., 2006. Multiscale Modeling of Gas-Fluidized Beds. Advances in Chemical Engineering 31, 65–149. https://doi.org/10.1016/S0065-2377(06)31002-2
- Wang, T.-J., Jin, Y., Tsutsumi, A., Wang, Z., Cui, Z., 2000. Energy transfer mechanism in a vibrating fluidized bed. Chemical Engineering Journal 78, 115–123. https://doi.org/10.1016/S1385-8947(00)00160-1
- Wu, K., de Martín, L., Coppens, M.-O., 2017. Pattern formation in pulsed gas-solid fluidized beds The role of granular solid mechanics. Chemical Engineering Journal 329, 4–14. https://doi.org/10.1016/j.cej.2017.05.152

- Xiang, L., Shuyan, W., Huilin, L., Goudong, L., Juhui, C., Yikun, L., 2010. Numerical simulation of particle motion in vibrated fluidized beds. Powder Technology 197, 25–35. https://doi.org/10.1016/j.powtec.2009.08.016
- Xu, Y., Musser, J., Li, T., Padding, J.T., Rogers, W.A., 2017. Particles climbing along a vertically vibrating tube: numerical simulation using the Discrete Element Method (DEM). Powder Technology 320, 304–312. https://doi.org/10.1016/j.powtec.2017.07.047
- Yang, W.-C., 2003. Handbook of Fluidization and Fluid-Particle Systems. CRC Press.
- Yang, X., Wang, S., Yang, J., Zhao, Y., 2023. Study on heterogeneous gas-solid structure and interparticle collision behavior in a vibrated fluidized bed of Geldart D particles using CFD-DEM simulations. Powder Technology 427, 118691. https://doi.org/10.1016/j.powtec.2023.118691
- Yang, X., Zhang, Y., Yang, Y., Zhou, E., Fu, Z., Zhao, Y., 2017. Fluidization of Geldart D type particles in a shallow vibrated gas-fluidized bed. Powder Technology 305, 333–339. https://doi.org/10.1016/j.powtec.2016.09.044
- Zeilstra, C., van der Hoef, M.A., Kuipers, J.A.M., 2008. Simulation of density segregation in vibrated beds. Phys. Rev. E 77, 031309. https://doi.org/10.1103/PhysRevE.77.031309
- Zhang, S., Ge, W., 2024. Accelerating discrete particle simulation of particle-fluid systems. Current Opinion in Chemical Engineering 43, 100989. https://doi.org/10.1016/j.coche.2023.100989